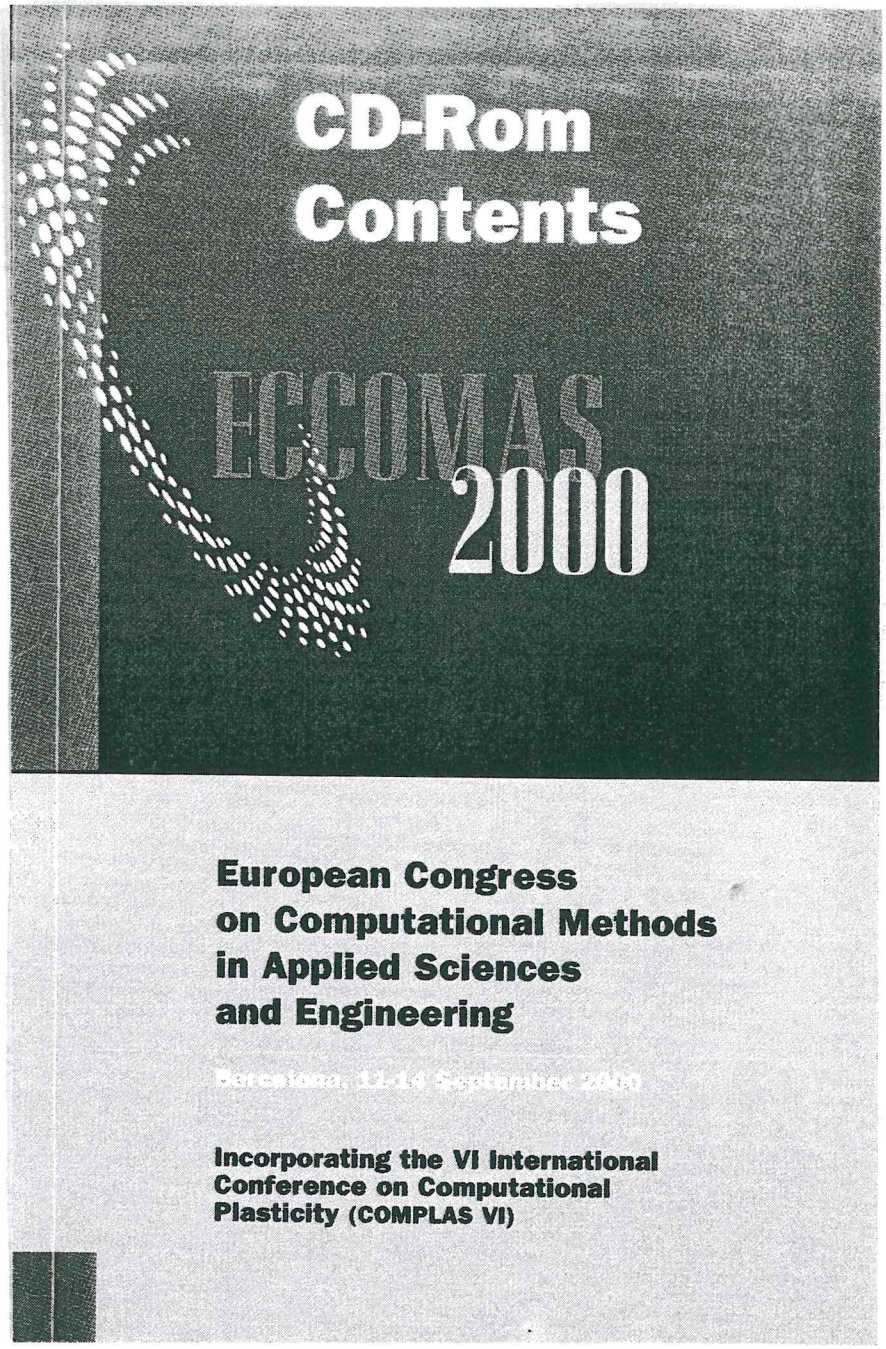

©ECCOMAS
European Community on
Computational Methods
in Applied Sciences

Cover design by: Jordi Palli

Printed by Artes Gráficas Torres S.A., Morales 17, 08029 Barcelona, Spain

Depósito legal: B-37139-2000

ISBN: 84-89925-70-4

European Congress on Computational Methods in Applied Sciences and Engineering
ECCOMAS 2000
Barcelona, 11-14 September 2000
©ECCOMAS

ON BIFURCATION IN LOCAL AND NONLOCAL MATERIALS WITH TENSION AND COMPRESSION DAMAGE

Claudia Comi° and Egidio Rizzi•

°Politecnico di Milano, Dipartimento di Ingegneria Strutturale,
piazza Leonardo da Vinci 32, I-20133 Milano, Italy
e-mail: comi@stru.polimi.it

•Politecnico di Bari, Facoltà di Ingegneria di Taranto,
Dipartimento di Ingegneria Strutturale, Via Orabona 4, I-70125 Bari, Italy
email: rizzi@stru.polimi.it

Key words: Continuum Damage Mechanics, tension/compression, concrete, strain localization, nonlocal integral damage, gradient-dependent damage.

Abstract. *In the present work an isotropic damage model for concrete accounting separately for progressive degradation of the elastic properties under prevailing tension and compression stress states is considered in both local and nonlocal forms. The possible occurrence of material instabilities in the form of strain localization is analyzed. For the local model, the bifurcation conditions at the onset of strain localization are first solved in terms of the critical values of the damage variables. Next, in order to avoid ill-posedness of the initial-boundary value problem, two nonlocal enhancements are provided through integral averaging or gradient dependency. The regularizing properties of both nonlocal formulations are explored. The expressions of the characteristic lengths implicitly introduced by the nonlocal enhancements are derived through a one-dimensional wave propagation analysis. Such results are confirmed by preliminary numerical FE simulations of the quasi-static response of a tensile bar analyzed with the nonlocal damage model.*

1 INTRODUCTION

The inelastic phenomena involved in the macroscopic behavior of quasi-brittle materials such as concrete and rocks can be modeled in the framework of Continuum Damage Mechanics. The available formulations of elastic-damage constitutive models cover a wide variety of material responses, such as for example damage-induced anisotropy and stiffness recovery due to microcrack closure upon stress reversal (unilateral damage). The formulation of elastic-damage models is often completed by coupling them to plasticity models in view of a comprehensive modeling of the material behavior under general two and three-dimensional stress states involving arbitrary degrees of confinement, when significant irreversible strains may be recorded after unloading. Among many others we quote here the models proposed in [1, 2, 3, 4, 5, 6, 7, 8].

In the present work we focus our attention to the modeling of pure elastic-damage in isotropic materials displaying different behaviors in tension/compression. A recently proposed isotropic damage model [9] is reconsidered. This model is characterized by the definition of two scalar damage variables, one devoted to describe damage due to prevailing tension stress states and the other accounting for damage under prevailing compression stress states. Two intersecting loading surfaces, both evolving with damage, define the current elastic domain in stress (or strain) space; nonlinear hardening/softening is governed by two damage functions, one for the tension and the other for the compression states, which possess in general an hardening branch followed by a softening post-peak tail. The material parameters are conveniently introduced to control separately the peak strengths and hardening/softening slopes for both the behaviors in tension and compression.

As widely studied, see e.g. [10, 11, 12, 13, 14], damage induced softening causes ill-posedness of the initial-boundary value problem and various regularization approaches have been proposed in the literature [15, 16, 17, 18, 19]. In this work, in view of regularizing the above described elastic-damage model, two different forms of nonlocal enrichment are considered, which give rise to the following two models: the first one is an integral nonlocal damage model in which the local strain invariants entering the loading functions are substituted by their spatially-weighted averages [19]; the second one is a gradient-enhanced damage model in which the loading functions are enriched as in [18] by adding extra-terms which contain the spatial laplacians of the damage variables. The conditions under which bifurcated solutions of the initial-boundary value problem become possible [20, 21, 22, 23, 24] are first established for the local damage model. Particular attention is devoted to the instabilities arising from loading paths inducing the activation of only one damage mechanism or the simultaneous activation of both damage mechanisms (namely from stress states sticked to the corners of the current elastic domain); the instability conditions are solved in terms of the critical values of the damage variables. Then, the two nonlocal models are considered and compared in terms of their regularizing properties and bifurcation predictions. Since two different damage mechanisms are present, two different

internal length scales (one relevant to tension and the other to compression stress states) are introduced by the nonlocal models. This seems to agree with experimental evidences on the post-peak behavior of concrete specimens under uniaxial tension and compression conditions, showing widths of the zones where the strains are highly localized which may be different of one order of magnitude in tension and compression [25, 26].

It is shown that both nonlocal enhancements allow to restore the well-posedness of the initial-boundary value problem and avoid strain localization into bands of vanishing width upon mesh refinement. Further insight into the regularizing properties of both nonlocal enhancements is given by a one-dimensional wave propagation analysis which allows to define the width of the localization zone. Quasi-static numerical FE simulations performed for this one-dimensional case with the nonlocal damage model are in agreement with the theoretical predictions.

2 BI-DISSIPATIVE LOCAL DAMAGE MODEL

The isotropic free energy density function ψ of the material is defined as

$$\psi = \psi(\boldsymbol{\varepsilon}, D_t, D_c) = \frac{1}{2}\left(2\mu\, \mathbf{e} : \mathbf{e} + K_+ \left(\mathrm{tr}^+ \boldsymbol{\varepsilon}\right)^2 + K_- \left(\mathrm{tr}^- \boldsymbol{\varepsilon}\right)^2\right) \tag{1}$$

with

$$\begin{cases} \mu \;\; = \mu_0 \;\; (1 - D_t)\,(1 - D_c) \\ K_+ = K_0 \;\; (1 - D_t)\,(1 - D_c) \\ K_- = K_0 \;\; (1 - D_c) \end{cases} \tag{2}$$

In eqns (1) and (2) D_t and D_c are the damage variables in tension and compression, respectively, both varying in the interval [0,1[, μ_0 is the initial shear modulus, K_0 is the initial bulk modulus, while μ, K_+ and K_- are their damaged counterparts, the latter two, respectively, in the tension ($\mathrm{tr}\,\boldsymbol{\varepsilon}>0$) and compression ($\mathrm{tr}\,\boldsymbol{\varepsilon}<0$) subdomains; $\boldsymbol{\varepsilon}$ is the small strain tensor and $\mathbf{e}$ is its deviatoric part. Symbols $\mathrm{tr}^+\boldsymbol{\varepsilon}$ and $\mathrm{tr}^-\boldsymbol{\varepsilon}$ denote the positive and negative parts of the trace of the strain tensor, $\mathrm{tr}\,\boldsymbol{\varepsilon}=\mathbf{I}:\boldsymbol{\varepsilon}$, where $\mathbf{I}$ is the 2nd-order identity tensor:

$$\mathrm{tr}^+\boldsymbol{\varepsilon} = \frac{\mathrm{tr}\,\boldsymbol{\varepsilon} + |\mathrm{tr}\,\boldsymbol{\varepsilon}|}{2}\,, \qquad \mathrm{tr}^-\boldsymbol{\varepsilon} = \frac{\mathrm{tr}\,\boldsymbol{\varepsilon} - |\mathrm{tr}\,\boldsymbol{\varepsilon}|}{2} \tag{3}$$

The stress tensor $\boldsymbol{\sigma}$ is given by the following state equation:

$$\boldsymbol{\sigma} = \left.\frac{\partial\psi}{\partial\boldsymbol{\varepsilon}}\right|_{D_t,D_c} = 2\mu\,\mathbf{e} + K_+\,\mathrm{tr}^+\boldsymbol{\varepsilon}\,\mathbf{I} + K_-\,\mathrm{tr}^-\boldsymbol{\varepsilon}\,\mathbf{I} \tag{4}$$

while a further differentiation renders the 4th-order secant stiffness tensor entering the secant stress/strain law $\boldsymbol{\sigma}=\mathbb{E}:\boldsymbol{\varepsilon}$,

$$\mathbb{E} = \left.\frac{\partial^2\psi}{\partial\boldsymbol{\varepsilon}\otimes\partial\boldsymbol{\varepsilon}}\right|_{D_t,D_c} = 2\mu\,\mathbb{P}_d + \Big(3K_+\,\mathcal{H}(\mathrm{tr}\,\boldsymbol{\varepsilon}) + 3K_-\,\mathcal{H}(-\mathrm{tr}\,\boldsymbol{\varepsilon})\Big)\,\mathbb{P}_v \tag{5}$$

where $\mathbb{P}_v = \mathbf{I}\otimes\mathbf{I}/3$ and $\mathbb{P}_d = \mathbb{I}^s - \mathbb{P}_v$ are the volumetric and deviatoric 4th-order projection operators, and $\mathbb{I}^s = \mathbf{I}\,\underline{\overline{\otimes}}\,\mathbf{I}$ is the 4th-order symmetric identity tensor, which is built from $\mathbf{I}$ through the symmetrized dyadic product $\underline{\overline{\otimes}}$; $\mathcal{H}(x)$ is the unit-step (Heavyside) function ($\mathcal{H}(x)=1$ if $x>0$, $\mathcal{H}(x)=0$ if $x<0$). The stiffness tensor $\mathbb{E}$ is endowed with both minor and major symmetries and is positive definite for all values of the damage variables in the range $[0,1[$ provided that the isotropic undamaged stiffness $\mathbb{E}_0 = 2\mu_0\ \mathbb{P}_d + 3K_0\ \mathbb{P}_v$ is positive definite, namely for $\mu_0>0$, $K_0>0$. Notice that bulk material properties and elastic stiffness (5) are not defined on the interface surface in strain space, $\mathrm{tr}\,\boldsymbol{\varepsilon}=0$ [27]. However, stress continuity at the interface is assured in (4), since $\mathrm{tr}\,\boldsymbol{\varepsilon}$ vanishes on the interface. Due to the fact that the material response is assumed isotropic, tension and compression subdomains of the elastic properties are separated in stress space by the dual interface surface $\mathrm{tr}\,\boldsymbol{\sigma}=0$. For this reason, the argument of the unit-step function in (5) can be equivalently taken as $\mathrm{tr}\,\boldsymbol{\sigma}$.

The damage activation and the evolution of the damage variables are governed by the following loading/unloading conditions:

$$f_t \le 0 \quad \dot{D}_t \ge 0 \quad f_t\,\dot{D}_t = 0\,; \qquad f_c \le 0 \quad \dot{D}_c \ge 0 \quad f_c\,\dot{D}_c = 0 \tag{6}$$

where f_t and f_c are two activation functions for states of prevailing tension or compression, respectively, which are defined in stress space as

$$\begin{aligned} f_t &= J_2(\boldsymbol{\sigma}) - a_t\, I_1^2(\boldsymbol{\sigma}) + b_t\, r_t(D_t)\ I_1(\boldsymbol{\sigma}) - k_t\, r_t^2(D_t)\ (1-\alpha D_c) \\ f_c &= J_2(\boldsymbol{\sigma}) + a_c\, I_1^2(\boldsymbol{\sigma}) + b_c\, r_c(D_c)\ I_1(\boldsymbol{\sigma}) - k_c\, r_c^2(D_c) \end{aligned} \tag{7}$$

In the above equations, $J_2(\boldsymbol{\sigma}) = \boldsymbol{\sigma}_d : \boldsymbol{\sigma}_d/2$ is the second invariant of the stress deviator $\boldsymbol{\sigma}_d = \mathbb{P}_d : \boldsymbol{\sigma}$, $I_1(\boldsymbol{\sigma}) = \mathrm{tr}\,\boldsymbol{\sigma}$ is the first invariant of the stress tensor, a_t, b_t, k_t, α, a_c, b_c, k_c are nonnegative material parameters ($a_t \le 1/3$), and r_t, r_c are two hardening/softening functions defined as follows

$$r_i(D_i) = \begin{cases} 1 - \dfrac{1-\left(\dfrac{\sigma_e}{\sigma_0}\right)_i}{D_{0_i}^2}\,(D_{0_i} - D_i)^2 & \text{for} \quad D_i < D_{0_i} \\[2ex] \left[1 - \left(\dfrac{D_i - D_{0_i}}{1 - D_{0_i}}\right)^{c_i}\right]^{3/4} & \text{for} \quad D_i \ge D_{0_i} \end{cases} \qquad i = t, c \tag{8}$$

where $c_i \ge 2$ are the softening exponents, and σ_{e_i} and σ_{0_i} denote the absolute stress values at first elastic limit and at peak under uniaxial stress conditions, while D_{0_i} are the corresponding values of the damage variables at peak. Due to such physical meaning, the material parameters are linked by the following relations:

$$(1/3 - a_t)\,\sigma_{0_t}^2 + b_t\,\sigma_{0_t} - k_t = 0\,, \quad (1/3 + a_c)\,\sigma_{0_c}^2 - b_c\,\sigma_{0_c} - k_c = 0 \tag{9}$$

The two damage conditions originate a vertex-like structure (two corners in case of plane stress) where they intersect in a region that lies, at the beginning of the damage process, on the compression side of the stress space $\mathrm{tr}\,\boldsymbol{\sigma}<0$. The two loading functions are conceived in a way apt to reproduce the typical shape of the concrete failure domain under biaxial stress states [9]. Functions (7) can be equivalently expressed in strain space in terms of the strain invariants $\mathrm{tr}\,\boldsymbol{\varepsilon}$ and $J_2^{\varepsilon}=\mathbf{e}:\mathbf{e}/2$, by using the relations

$$J_2\left(\boldsymbol{\sigma}\right)=\frac{1}{2}\,\boldsymbol{\sigma}_d:\boldsymbol{\sigma}_d=4\mu^2\,J_2^{\varepsilon}\;,\qquad I_1\left(\boldsymbol{\sigma}\right)=\mathrm{tr}\,\boldsymbol{\sigma}=3K_+\,\mathrm{tr}^+\,\boldsymbol{\varepsilon}+3K_-\,\mathrm{tr}^-\,\boldsymbol{\varepsilon} \tag{10}$$

which arise from the isotropic stress/strain relation (4) involving decoupling of deviatoric, $\boldsymbol{\sigma}_d=2\mu\,\mathbf{e}$, and volumetric $(10)_b$ responses.

3 BIFURCATION ANALYSIS OF THE LOCAL MODEL

Differentiation with respect to time of the secant stress/strain law $\boldsymbol{\sigma}=\mathbb{E}:\boldsymbol{\varepsilon}$ yields

$$\dot{\boldsymbol{\sigma}}=\mathbb{E}:\dot{\boldsymbol{\varepsilon}}\;+\mathbf{M}_t\,\dot{D}_t+\mathbf{M}_c\,\dot{D}_c \tag{11}$$

where

$$\mathbf{M}_t=\left.\frac{\partial\mathbb{E}}{\partial D_t}\right|_{\boldsymbol{\varepsilon}}:\boldsymbol{\varepsilon}=-\left(1-D_c\right)\left(2\mu_0\,\mathbf{e}+K_0\,\mathrm{tr}^+\,\boldsymbol{\varepsilon}\,\mathbf{I}\right)=-\frac{\boldsymbol{\sigma}_d+\mathrm{tr}^+\boldsymbol{\sigma}\,\mathbf{I}/3}{\left(1-D_t\right)} \tag{12}$$

$$\mathbf{M}_c=\left.\frac{\partial\mathbb{E}}{\partial D_c}\right|_{\boldsymbol{\varepsilon}}:\boldsymbol{\varepsilon}=-\left(1-D_t\right)\left(2\mu_0\,\mathbf{e}+K_0\,\mathrm{tr}^+\,\boldsymbol{\varepsilon}\,\mathbf{I}\right)+K_0\,\mathrm{tr}^-\,\boldsymbol{\varepsilon}\,\mathbf{I}=-\frac{\boldsymbol{\sigma}}{\left(1-D_c\right)} \tag{13}$$

Assuming loading in the inelastic range for both dissipation mechanisms, from the consistency conditions $\dot{f}_t=0$ and $\dot{f}_c=0$, $\dot{D}_t$ and $\dot{D}_c$ can be solved in terms of $\dot{\boldsymbol{\varepsilon}}$ and back-substituted in (11) to obtain the tangent stiffness of the rate relation $\dot{\boldsymbol{\sigma}}=\mathbb{E}_T:\dot{\boldsymbol{\varepsilon}}$, namely:

$$\mathbb{E}_T=\mathbb{E}+\frac{\mathbf{M}_t\otimes\left(H_{cc}\mathbf{N}_t-H_{tc}\mathbf{N}_c\right)}{H}+\frac{\mathbf{M}_c\otimes\left(-H_{ct}\mathbf{N}_t+H_{tt}\mathbf{N}_c\right)}{H} \tag{14}$$

where

$$\mathbf{N}_t=\left.\frac{\partial f_t}{\partial\boldsymbol{\varepsilon}}\right|_{D_t,D_c}=2\mu\,\boldsymbol{\sigma}_d+\left[b_t\,r_t(D_t)-2a_t\,\mathrm{tr}\,\boldsymbol{\sigma}\right]\left[3K^+\,\mathcal{H}(\mathrm{tr}\,\boldsymbol{\sigma})+3K^-\,\mathcal{H}(-\mathrm{tr}\,\boldsymbol{\sigma})\right]\mathbf{I} \tag{15}$$

$$\mathbf{N}_c=\left.\frac{\partial f_c}{\partial\boldsymbol{\varepsilon}}\right|_{D_t,D_c}=2\mu\,\boldsymbol{\sigma}_d+\left[b_c\,r_c(D_c)+2a_c\,\mathrm{tr}\,\boldsymbol{\sigma}\right]\left[3K^+\,\mathcal{H}(\mathrm{tr}\,\boldsymbol{\sigma})+3K^-\,\mathcal{H}(-\mathrm{tr}\,\boldsymbol{\sigma})\right]\mathbf{I} \tag{16}$$

and H_{ij} and H are the components and the determinant of the 2×2 nonsymmetric hardening matrix $\mathbf{H}$

$$\mathbf{H}=\begin{bmatrix}H_{tt} & H_{tc}\\ H_{ct} & H_{cc}\end{bmatrix}=-\begin{bmatrix}\left.\dfrac{\partial f_t}{\partial D_t}\right|_{\boldsymbol{\varepsilon}} & \left.\dfrac{\partial f_t}{\partial D_c}\right|_{\boldsymbol{\varepsilon}}\\ \left.\dfrac{\partial f_c}{\partial D_t}\right|_{\boldsymbol{\varepsilon}} & \left.\dfrac{\partial f_c}{\partial D_c}\right|_{\boldsymbol{\varepsilon}}\end{bmatrix}\;;\qquad H=\det\mathbf{H} \tag{17}$$

which is assumed to be positive definite. The tangent stiffness $\mathbb{E}_T$, eqn (14), is obtained by two rank-one updates of the elastic stiffness $\mathbb{E}$ [24]. However, if only one damage mechanism is active, either in tension or in compression, only a single rank-one update modifies the damaged elastic stiffness:

$$\mathbb{E}_T = \mathbb{E} + \frac{\mathbf{M}_i \otimes \mathbf{N}_i}{H_{ii}} \,, \quad i = t \text{ or } c \tag{18}$$

Following [21, 22], the onset of strain localization in the material element is sought as a bifurcation of the strain rate across a surface of local normal $\mathbf{n}$ and is signaled by the first singularity of the 2nd-order acoustic tensor $\mathbf{Q}_T$:

$$\mathbf{Q}_T = \mathbf{n} \cdot \mathbb{E}_T \cdot \mathbf{n} \,, \qquad \det \mathbf{Q}_T = 0 \tag{19}$$

where, in turn, $\mathbf{Q}_T$ is obtained from one or two rank-one updates of the (positive definite) elastic acoustic tensor $\mathbf{Q}$=$\mathbf{n}\cdot\mathbb{E}\cdot\mathbf{n}$. Analytical solutions of the localization condition $(19)_b$ have been provided for various material models in terms of critical hardening moduli and critical localization directions, see e.g. [20, 12, 23, 24, 28].

The onset of bifurcation has been investigated for different biaxial stress paths in the plane $(\sigma_1, \sigma_2, \sigma_3{=}0)$ comprising: radial stress paths at fixed σ_1/σ_2 ratios, and stress paths sticked to the corner of the biaxial elastic domain at the intersection f_t=0, f_c=0. The latter hardening/softening paths are driven by damage activation of a single mechanism only, in tension (D_c=0), or compression (D_t=0), or by simultaneous activation of both damage mechanisms (D_t=D_c). The pure shear radial paths are slightly on the positive or negative sides of the interface bisector line $\sigma_2{=}{-}\sigma_1$. In the strain localization analysis, the following material parameters have been used: E_0=31000 MPa, ν_0=0.15; a_t=0.27, b_t=3.64 MPa, k_t=12.2 MPa^2, $\sigma_{e_t}/\sigma_{0_t}$=0.8, c_t=5., D_{0_t}=0.1, α=1.; a_c=0.003, b_c=2.804 MPa, k_c=233.4 MPa^2, $\sigma_{e_c}/\sigma_{0_c}$=0.7, c_c=5., D_{0_c}=0.3, which, from eqn (9), correspond to a concrete with uniaxial peak stresses σ_{0_t}=3.18 MPa and σ_{0_c}=30.84 MPa, and, for the different peak stress points of the biaxial failure domain: in equibiaxial tension (1/1) $\sigma_{0_{tt}}$=2.15 MPa, in equibiaxial compression (−1/−1) $\sigma_{0_{cc}}$=35.36 MPa, in pure shear (−1/1) σ_{0_s}=3.49 MPa, and at the corner $\sigma_{0_{1c}}$=−29.28 MPa, $\sigma_{0_{2c}}$=2.07 MPa. During hardening/softening the corner always lies on the compression side $\operatorname{tr}\boldsymbol{\sigma}<0$ of the stress plane.

Figures 1,2 report the localization index defined as the normalized determinant of the acoustic tensor, $\det \mathbf{Q}_T/\det \mathbf{Q}$, as a function of the inclination angle θ between the normal $\mathbf{n}$ and the principal stress direction 1. The normal to the localization surface may lie In-Plane (IP) of principal stress directions (1,2), or Out-Plane (OP), possibly belonging to a cone of localization normals with axis 3 orthogonal to that plane. Such occurrence depends on the relative positions of the max./min. and intermediate principal stresses of the stress deviator. Critical localization directions and hardening parameters have been determined by using a geometrical method [28], and solved for the critical damage threshold values. The corresponding results are gathered in Table 1 below.

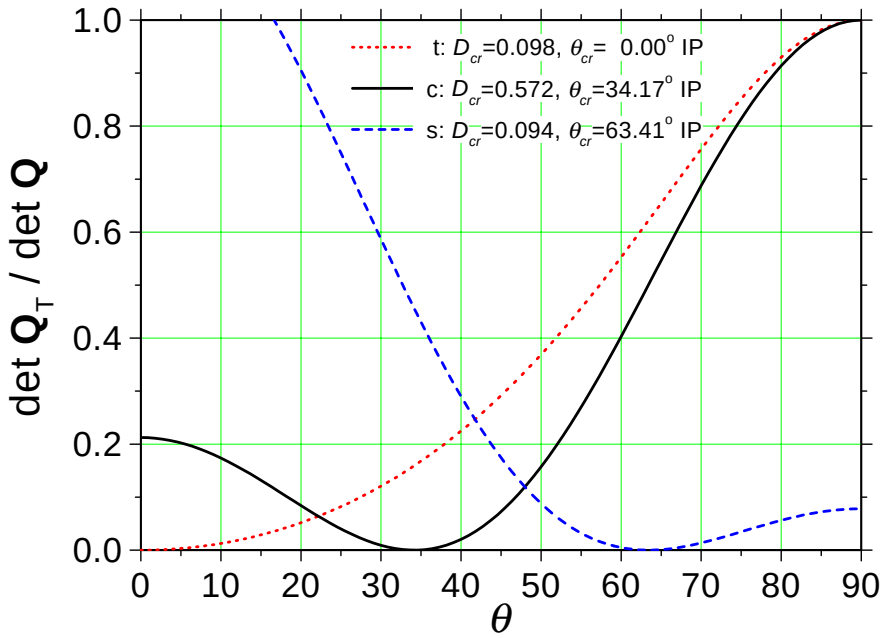

Figure 1: Localization index for t: uniaxial tension, c: uniaxial compression and s: pure shear. Critical damage D_{cr} and In-Plane (IP) inclination θ_{cr} of the localization normal.

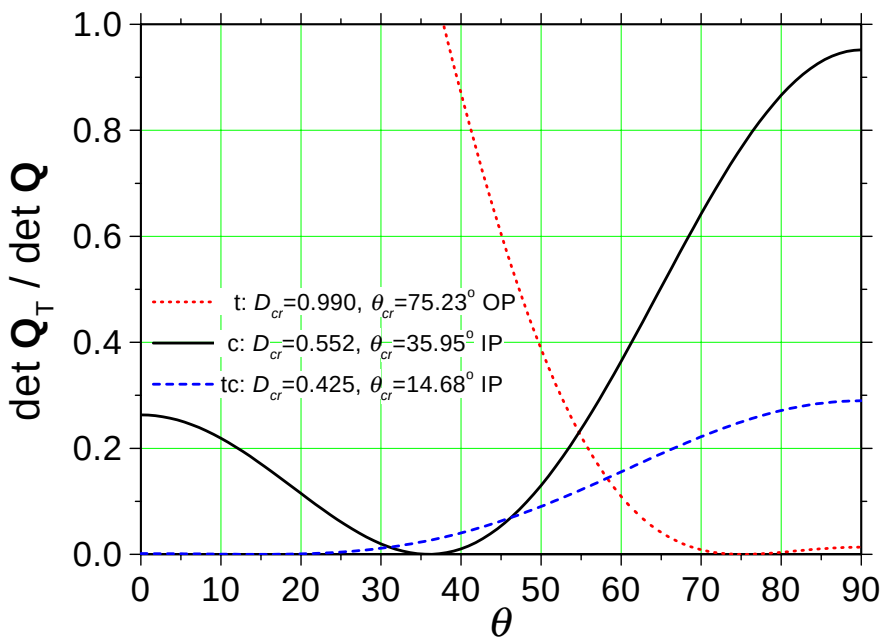

Figure 2: Localization index for a stress state sticked to the corner of the biaxial stress domain; active damage mechanisms in t: tension with D_c=0, c: compression with D_t=0, tc: tension and compression on the radial damage path D_t=D_c. Critical damage D_{cr} and In-Plane (IP) or Out-Plane (OP) inclination θ_{cr} of the localization normal.

Figure 1 shows the localization index for the paths of uniaxial tension and compression, and for pure shear on the tension side of the elastic domain. In these three cases localization is detected in plane (for the uniaxial cases the normal actually belongs to a cone with axis along principal stress direction 1). Due to nonassociativity, in uniaxial tension and pure shear strain localization occurs in the hardening regime for a critical damage value which is slightly below the peak stress damage D_{0_t}=0.1. In uniaxial compression instead, localization occurs in the softening range, after the damage value D_{0_c}=0.3 has been overcome. In uniaxial tension the localization normal is aligned with the tensile axis, while it is inclined for the two other cases. In pure shear nonassociativity also induces a sort of 'acceleration effect' [24] with $\det \mathbf{Q}_T / \det \mathbf{Q}$ overcoming 1 for certain directions.

Figure 2 depicts the normalized determinant of the acoustic tensor for stress states sticked at the corner. When damage evolves only in tension localization is detected out of plane and only very near the limit value D_t=1. The max. and intermediate principal stresses of the stress deviator shift position only after D_t=0.9, so that out-of-plane localization becomes possible. For certain directions the 'acceleration effect' is also significantly present. The compression-active corner shows a profile with features similar to those of the uniaxial compression case and localization in the softening range. When both damage mechanisms are co-present the triggering effect of strain localization is apparent: the corner activation and the corresponding double rank-one update destabilizes the tangent stiffness and consequently the acoustic tensor. Localization occurs when both mechanisms are in the softening range for damage values preceding the critical values for singly-active damage mechanisms. The profile of the localization index is also flattened-out with a reduced gap between valleys and peaks.

The other biaxial stress paths reported in Table 1 displayed similar features: in equibiaxial tension and compression, localization happens in the softening range and occurs out of plane on a cone with axis perpendicular to the stress plane. Pure shear on the compression side shows only minor variations due to the slight differences in elastic moduli that produce at the low damage values where localization takes place right before peak.

Stress and damage paths	Critical damage	Localization direction
equibiaxial tension	$D_{t_{cr}} = 0.793$	$\theta_{cr} = 10.10°$ (OP)
uniaxial tension	$D_{t_{cr}} = 0.098$	$\theta_{cr} = 0.00°$ (IP)
pure shear in tension domain	$D_{t_{cr}} = 0.094$	$\theta_{cr} = 63.41°$ (IP)
pure shear in compression domain	$D_{t_{cr}} = 0.094$	$\theta_{cr} = 63.89°$ (IP)
corner with t. path D_c=0	$D_{t_{cr}} = 0.990$	$\theta_{cr} = 75.23°$ (OP)
corner with c. path D_t=0	$D_{c_{cr}} = 0.552$	$\theta_{cr} = 35.95°$ (IP)
corner with t./c. path D_t=D_c	$D_{cr} = 0.425$	$\theta_{cr} = 14.68°$ (IP)
uniaxial compression	$D_{c_{cr}} = 0.571$	$\theta_{cr} = 34.17°$ (IP)
equibiaxial compression	$D_{c_{cr}} = 0.753$	$\theta_{cr} = 40.51°$ (OP)

Table 1: Results of strain localization analysis for different biaxial stress paths.

4 ENHANCED MODELS

4.1 Model with nonlocal integral enhancement

As proposed in [19], a nonlocal model can be obtained by introducing in the loading functions (7), expressed in strain space through eqns (10), the following nonlocal strain measures at a point $\mathbf{x}$ of the solid

$$\langle J_2^{\varepsilon}(\mathbf{x})\rangle = \int_V W(\mathbf{x}-\mathbf{s})\, J_2^{\varepsilon}(\mathbf{s})\, dV \tag{20}$$

$$\left\langle tr^+ \boldsymbol{\varepsilon}(\mathbf{x})\right\rangle = \int_V W(\mathbf{x}-\mathbf{s})\, tr^+ \boldsymbol{\varepsilon}(\mathbf{s})\, dV \ , \quad \left\langle tr^- \boldsymbol{\varepsilon}(\mathbf{x})\right\rangle = \int_V W(\mathbf{x}-\mathbf{s})\, tr^- \boldsymbol{\varepsilon}(\mathbf{s})\, dV \tag{21}$$

where dV is the volume element at point $\mathbf{s}$ and $W(\mathbf{x}-\mathbf{s})$ is the weighting function, here assumed as the normalized Gauss function

$$W(\mathbf{x}-\mathbf{s}) = \frac{\exp\left(-\dfrac{\|\mathbf{x}-\mathbf{s}\|^2}{2\,l^2}\right)}{\displaystyle\int_V \exp\left(-\dfrac{\|\mathbf{x}-\mathbf{s}\|^2}{2\,l^2}\right) dV} \tag{22}$$

Note that the averages (20)-(21) are extended to the whole volume V, but due to the shape of the weighting function (22), the material parameter l, with dimension of a length, defines in practice the region of the body surrounding point $\mathbf{x}$ which really influences the behavior at that point.

To take into account the different behaviors of concrete-like materials concerning localized phenomena in tension and compression, two different length parameters, l_t and l_c, can be used in (20)-(22) to perform the averages of the strain invariants to be introduced in the loading functions. Denoting by $\langle\circ\rangle_t$ and $\langle\circ\rangle_c$ the averages of quantity $\circ$ performed with l_t and l_c, respectively, the resulting nonlocal yield functions F_t and F_c are obtained by substituting to the local strain invariants their average values:

$$\begin{aligned} F_t &= 4\mu^2 \langle J_2^{\varepsilon}\rangle_t - 9a_t \left(K_+ \left\langle tr^+ \boldsymbol{\varepsilon}\right\rangle_t + K_- \left\langle tr^- \boldsymbol{\varepsilon}\right\rangle_t\right)^2 \\ &\quad + 3b_t\, r_t(D_t) \left(K_+ \left\langle tr^+ \boldsymbol{\varepsilon}\right\rangle_t + K_- \left\langle tr^- \boldsymbol{\varepsilon}\right\rangle_t\right) - k_t\, r_t^2(D_t)\,(1-\alpha D_c) \\ F_c &= 4\mu^2 \langle J_2^{\varepsilon}\rangle_c + 9a_c \left(K_+ \left\langle tr^+ \boldsymbol{\varepsilon}\right\rangle_c + K_- \left\langle tr^- \boldsymbol{\varepsilon}\right\rangle_c\right)^2 \\ &\quad + 3b_c\, r_c(D_c) \left(K_+ \left\langle tr^+ \boldsymbol{\varepsilon}\right\rangle_c + K_- \left\langle tr^- \boldsymbol{\varepsilon}\right\rangle_c\right) - k_c\, r_c^2(D_c) \end{aligned} \tag{23}$$

As shown in [29, 19], strain localization into a band of zero width, which occurs in the local medium when condition $(19)_b$ is fulfilled, cannot occur in the nonlocal medium. In fact in this latter medium, the bifurcation condition is given by the singularity of a tensor (similar to the acoustic tensor of the local medium, eqn $(19)_a$) which depends on

the wavelength through the Fourier transform of the weighting function. This tensor coincides with the elastic acoustic tensor when the wavelength tends to zero and hence is nonsingular. Therefore the ill-posedness of the boundary value problem is avoided by this nonlocal enhancement.

4.2 Model with gradient-dependent enhancement

An alternative nonlocal model can be obtained by introducing the spatial gradients of the damage variables in the stress-based loading functions f_t and f_c, eqn (7). If only second-order gradients are included one has:

$$\begin{aligned} F_t &= f_t(\boldsymbol{\sigma}, D_t, D_c) + g_t^2\, G_t\,(D_t)\ \nabla^2 D_t \\ F_c &= f_c(\boldsymbol{\sigma}, D_c) + g_c^2\, G_c\,(D_c)\ \nabla^2 D_c \end{aligned} \tag{24}$$

where g_t and g_c are the diffusion coefficients, in tension and compression, with the dimensions of a force per unit length, and $G_t\,(D_t)$, $G_c\,(D_c)$ are the nondimensional diffusion functions. The functional dependence of G_t, G_c on damage is not specified here and will be discussed in Section 5.2. At this stage we only assume that these functions are positive for any value of the damage variables. Standard arguments (see e.g. [30]), summarized below, allow to prove that with this definitions the boundary value problem remains elliptic also in the softening regime.

Consider the quasi-static rate problem, assuming full loading conditions ($\dot{F}_t$=0 and $\dot{F}_c$=0):

$$\dot{\boldsymbol{\varepsilon}} = \frac{1}{2}\ \left(\nabla\dot{\mathbf{u}}+\nabla^T\dot{\mathbf{u}}\right)\ , \qquad \operatorname{div}\dot{\boldsymbol{\sigma}} = \mathbf{0} \tag{25}$$

$$\begin{aligned} \dot{F}_t = \frac{\partial f_t}{\partial \boldsymbol{\sigma}} : \dot{\boldsymbol{\sigma}} + \left[b_t\, I_1\,(\boldsymbol{\sigma}) - 2k_t\, r_t\,(D_t)\,(1-\alpha D_c)\right]\ r_t'(D_t)\,\dot{D}_t \\ +\ g_t^2\, G_t'(D_t)\,\nabla^2 D_t\ \dot{D}_t + g_t^2\ G_t\,(D_t)\,\nabla^2\dot{D}_t + \alpha k_t\, r_t^2\,(D_t)\,\dot{D}_c = 0 \end{aligned} \tag{26}$$

$$\begin{aligned} \dot{F}_c = \frac{\partial f_c}{\partial \boldsymbol{\sigma}} : \dot{\boldsymbol{\sigma}} + \left[b_c\, I_1\,(\boldsymbol{\sigma}) - 2k_c\, r_c\,(D_c)\right]\ r_c'(D_c)\,\dot{D}_c \\ +\ g_c^2\, G_c'(D_c)\,\nabla^2 D_c\ \dot{D}_c + g_c^2\ G_c\,(D_c)\,\nabla^2\dot{D}_c = 0 \end{aligned} \tag{27}$$

where $r_i'(D_i)$, $G_i'(D_i)$, are the first derivatives of functions $r_i(D_i)$, $G_i(D_i)$, i=t, c. The stress and strain increments can be eliminated from eqns (11) and (25). The symbol of the principal part of the system of eqns $(25)_b$,(26),(27) in the unknown rates $\dot{\mathbf{u}}$, $\dot{D}_t$, $\dot{D}_c$ is the array $\mathbf{S}\,(\tilde{\mathbf{n}})$

$$\mathbf{S}\,(\tilde{\mathbf{n}}) = \begin{bmatrix} \tilde{\mathbf{n}}\cdot\mathbb{E}\cdot\tilde{\mathbf{n}} & \mathbf{0} & \mathbf{0} \\ \mathbf{0} & g_t^2 G_t\,(D_t)\,\tilde{\mathbf{n}}\cdot\tilde{\mathbf{n}} & 0 \\ \mathbf{0} & 0 & g_c^2 G_c\,(D_c)\,\tilde{\mathbf{n}}\cdot\tilde{\mathbf{n}} \end{bmatrix} \tag{28}$$

The rate problem looses ellipticity whenever $\det\mathbf{S}\,(\tilde{\mathbf{n}})$=0 for some direction $\tilde{\mathbf{n}}\neq\mathbf{0}$, i.e. when

$$\det\left(\tilde{\mathbf{n}}\cdot\mathbb{E}\cdot\tilde{\mathbf{n}}\right)\ \left[g_t^2\, G_t\,(D_t)\,\tilde{\mathbf{n}}\cdot\tilde{\mathbf{n}}\right]\ \left[g_c^2\, G_c\,(D_c)\,\tilde{\mathbf{n}}\cdot\tilde{\mathbf{n}}\right] = 0 \tag{29}$$

This condition may be alternatively stated by seeking harmonic solutions of the system $(25)_b$,(26),(27) in the form of the rates $\dot{\mathbf{u}}$, $\dot{D}_t$, $\dot{D}_c \propto \exp(i\,\tilde{\mathbf{n}}\cdot\mathbf{x})$, with $\tilde{\mathbf{n}}=q\,\mathbf{n}$, q being the wave number and $\mathbf{n}$ a unit direction. Since the damaged elastic acoustic tensor $\mathbf{n}\cdot\mathbb{E}\cdot\mathbf{n}$ is positive definite, from (29) one can conclude that the problem remains elliptic for any $g_t^2\,G_t\,(D_t)>0$ and $g_c^2\,G_c\,(D_c)>0$.

5 ONE-DIMENSIONAL WAVE PROPAGATION ANALYSIS

Differences and similarities of the proposed models can be appreciated in the dynamic context by considering a one-dimensional wave propagation analysis: focusing only on the tensile behavior (the subindex $_t$ is dropped in the following), the model description can be simplified to:

$$\sigma = E_0\,(1-D)\,\varepsilon\ , \quad F = F_t \leq 0\ , \quad \dot{D} \geq 0\ , \quad F\dot{D} = 0 \tag{30}$$

where E_0 is the undamaged Young's modulus. Let us consider the one-dimensional equations of motion linearized around a strained homogeneous state (ε, D):

$$\dot{\sigma}_{,x} = \rho\ \ddot{u}\ , \qquad \dot{\sigma} = E_0\left[(1-D)\,\dot{u}_{,x} - \dot{D}\,\varepsilon\right]\ , \qquad \dot{F} = 0 \tag{31}$$

where ρ is the mass density of the bar. Starting from this homogeneous state, consider an harmonic wave of frequency ω and wave number q propagating through an enhanced damage bar with velocity and damage fields of the form:

$$\dot{u} = v_0 \exp\left(i\,(qx-\omega t)\right)\ , \qquad \dot{D} = d_0 \exp\left(i\,(qx-\omega t)\right) \tag{32}$$

5.1 Analysis with the nonlocal model

For the integral model of Section 4.1, specialized to the one-dimensional case, the consistency condition $(31)_c$ reads:

$$\dot{F} = (1-D)\ \frac{A(\varepsilon,D)}{\varepsilon}\int_L W\,(x-s)\,\dot{\varepsilon}\,(s)\,ds - \left[A(\varepsilon,D) + B(\varepsilon,D)\,r'(D)\right]\dot{D}\ =\ 0 \tag{33}$$

where the functions $A\,(\varepsilon,D)$, $B\,(\varepsilon,D)$ are defined as

$$A\,(\varepsilon,D) = 2\,(1/3-a)\,(1-D)\,E_0^2\,\varepsilon^2 + E_0\,\varepsilon\,b\,r\,(D) \tag{34}$$

$$B\,(\varepsilon,D) = 2\,k\,r\,(D) - (1-D)\,E_0\,\varepsilon\,b \tag{35}$$

Direct substitution of (32) into the linearized equations of motion (31), with $\dot{F}$ given by (33), yields a dependency of the phase velocity on the wave number q. The phase velocity for the nonlocal integral model is:

$$c_f = \frac{\omega}{q} = c_e\,\sqrt{\frac{A\,(\varepsilon,D)\left[1-\bar{W}\,(q)\right] + B\,(\varepsilon,D)\ r'(D)}{A\,(\varepsilon,D) + B\,(\varepsilon,D)\ r'(D)}} \tag{36}$$

where c_e is the elastic propagation velocity in the damaged bar

$$c_e = \sqrt{\frac{(1-D)\,E_0}{\rho}} \tag{37}$$

and $\bar{W}(q)$ is the Fourier transform of the Gauss function $W(x-s)$, eqn (22), rigorously only under the hypothesis that $L\to\infty$:

$$\bar{W}(q) = \int_{-\infty}^{+\infty} W(\xi)\,\exp(-i\,q\,\xi)\,d\xi = \exp\left(-\frac{q^2 l^2}{2}\right) \tag{38}$$

The phase velocity (36) is real if the wave number is such that the numerator of the term under square root in (36) is positive (which implies a positive denominator term $A+B\,r'$). This is always the case in the hardening regime ($r'(D)>0$), i.e. for $D<D_0$. On the contrary, for $D>D_0$, only waves with wavelength $\lambda\leq\lambda_{cr}$ do propagate, where

$$\lambda_{cr}=\frac{2\pi}{q_{cr}}=\sqrt{2}\pi l\left[-\ln\left(1+\frac{B(\varepsilon,D)}{A(\varepsilon,D)}\,r'(D)\right)\right]^{-0.5}=\sqrt{2}\pi l\left[-\ln\left(1+\frac{(1-D)}{r(D)}\,r'(D)\right)\right]^{-0.5} \tag{39}$$

and in the last equality the condition $F=0$ has been used. Since, due to the material dissipative behavior, high frequencies are damped, one obtains a stationary harmonic localization wave of wavelength λ_{cr}; this length represents the internal localization length. Note that this internal length turns out to be a decreasing function of the damage D. For $D=D_0$ the critical wavelength is infinite, while as $D\to 1$, the internal length tends to a finite nonzero value which can be computed from eqn (39). For example, assuming $D_0=0$, in $(8)_2$ one has

$$\lim_{D\to 1}\lambda_{cr} = \sqrt{2}\pi l\,[-\ln(0.25)]^{-0.5} = 3.773\,l \tag{40}$$

The evolution of the internal length λ_{cr} with damage D for varying material parameters l, c and D_0 is shown in Figs 3a,b,c, respectively. The thicker black curve in the three figures corresponds to the same set of material parameters. From Fig. 3a it can be observed that the material length l, according to eqn (39), equally affects the internal length for all damage values. On the contrary, a change of the exponent c of the softening branch does not affect the internal length at the limit $D\to 1$, see Fig. 3b. The curves for varying D_0 in Fig. 3c have vertical asymptotes at $D=D_0$; in fact, in the one-dimensional case localization takes place at the peak of the stress-strain curve (i.e. for $D=D_0$) and only after this value the characteristic length needs to be considered.

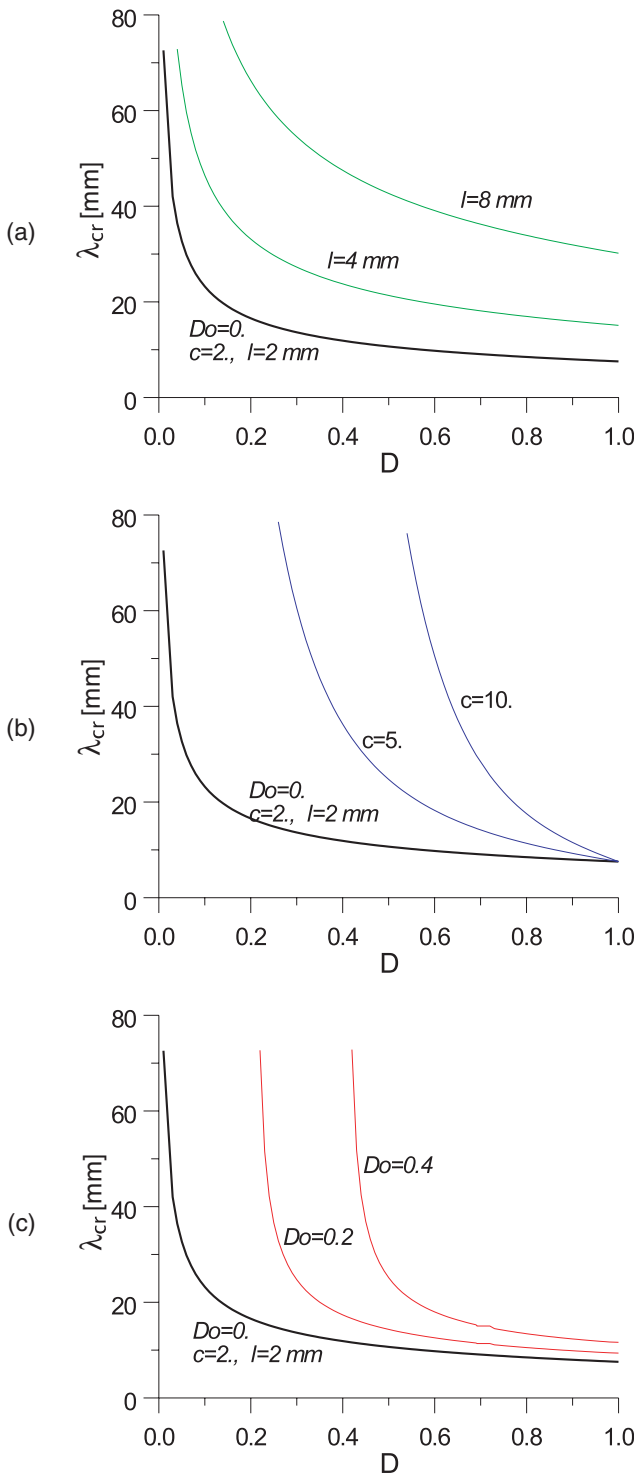

Figure 3: Evolution of the characteristic length λ_{cr} with damage D for: (a) varying length parameter l; (b) varying softening exponent c; (c) varying damage at peak D_0.

5.2 Analysis with the gradient-dependent model

Adopting a gradient-dependent formulation, from $(24)_1$ the consistency condition reads

$$\dot{F} = (1-D)\,\frac{A(\varepsilon,D)}{\varepsilon}\,\dot{\varepsilon} - [A(\varepsilon,D) + B(\varepsilon,D)\,r'(D)]\,\dot{D} + g^2\,G(D)\,\nabla^2\dot{D} = 0 \tag{41}$$

where functions $A(\varepsilon,D)$, $B(\varepsilon,D)$ are defined by eqns (34)-(35) and term $g^2\,\nabla^2 D\,G'(D)\,\dot{D}$ has been dropped due to the assumed homogeneity of the starting state.

Substituting the velocity fields (32) into the linearized equations of motion (31), with $\dot{F}$ now given by (41), yields again a dispersive relation between phase velocity c_f and wave number q. The phase velocity for the gradient-dependent model is:

$$c_f = \frac{\omega}{q} = c_e\,\sqrt{\frac{B\,(\varepsilon,D)\;r'(D) + g^2\,G\,(D)\,q^2}{A\,(\varepsilon,D) + B\,(\varepsilon,D)\;r'(D) + g^2\,G\,(D)\,q^2}} \tag{42}$$

where c_e is defined by eqn (37). The phase velocity (42) is real in the hardening regime and in the softening regime ($D{>}D_0$) if the wave number is such that the numerator is positive; this means that only waves with wavelength $\lambda{\leq}\lambda_{cr}$ do propagate, where

$$\lambda_{cr} = \frac{2\pi}{q_{cr}} = 2\pi\,\sqrt{\frac{g^2\,G\,(D)}{-B\,(\varepsilon,D)\;r'(D)}} \tag{43}$$

Using the condition $F{=}0$, and assuming for simplicity $a{=}1/3$, one obtains

$$\lambda_{cr} = \frac{2\pi}{q_{cr}} = 2\pi\,\frac{g}{\sqrt{k}}\,\sqrt{\frac{G\,(D)}{-r\,(D)\;r'(D)}} \tag{44}$$

Comparing this internal length with the one obtained for the integral model one may observe that the coefficient $g/\sqrt{k}$, with dimension of a length, plays the same role of $l/\sqrt{2}$ in eqn (39). In the gradient dependent model the internal length is also a function of damage and the evolution with damage depends on the chosen function $G\,(D)$. Four alternatives have been considered and the results in terms of the critical length evolution are shown in Fig. 4:

$$\text{model A}: \quad G\,(D) = 1 \tag{45}$$

$$\text{model B}: \quad G\,(D) = r(D) \tag{46}$$

$$\text{model C}: \quad G\,(D) = \left(1 - \left(\frac{D-D_0}{1-D_0}\right)^c\right)^{0.5} \quad \text{for } D > D_0 \tag{47}$$

$$\text{model D}: \quad G\,(D) = -r(D)\,r'(D) \tag{48}$$

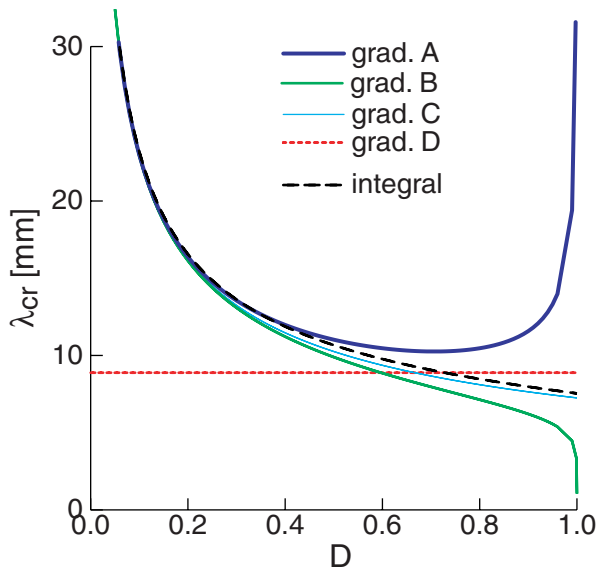

Figure 4: Evolution of the characteristic length λ_{cr} with damage D for the different enhanced models (D_0=0).

Model A, which corresponds to a constant coefficient of the gradient term and represents the simplest choice, leads to a critical wave length which tends to infinity both for D=D_0 and D→1 (blue bold curve in Fig. 4). This unbounded increase of the internal length as damage approaches these critical values is clearly unphysical.

On the contrary, with model B the internal length tends to zero as D tends to one (green curve of Fig. 4). This allows to model the transition from a localization zone to a macrocrack; however numerical problems may be encountered for high values of damage and adaptive mesh refinement or transition from a continuous approach to a discontinuous one would be required.

With model C one obtains a behavior which is very similar to the one observed for the nonlocal model: compare the light blue curve with the black dashed curve of Fig. 4 obtained by the gradient model and the integral model, respectively, with parameters $g/\sqrt{k}$=$l/\sqrt{2}$.

Finally, a constant internal length is obtained with the last choice (model D). Other different curves could of course be obtained for different choices of $G\,(D)$, the only constraint on this function being its positiveness for any $0\leq D<1$.

6 NUMERICAL TEST WITH THE NONLOCAL DAMAGE MODEL

Numerical simulations require time and space discretizations. In this work a backward difference integration scheme of the nonlocal constitutive model of Section 4.1 is adopted and space discretization is performed following a standard displacement-based approach. Due to the particular form of nonlocality adopted, in which only the strain invariants are

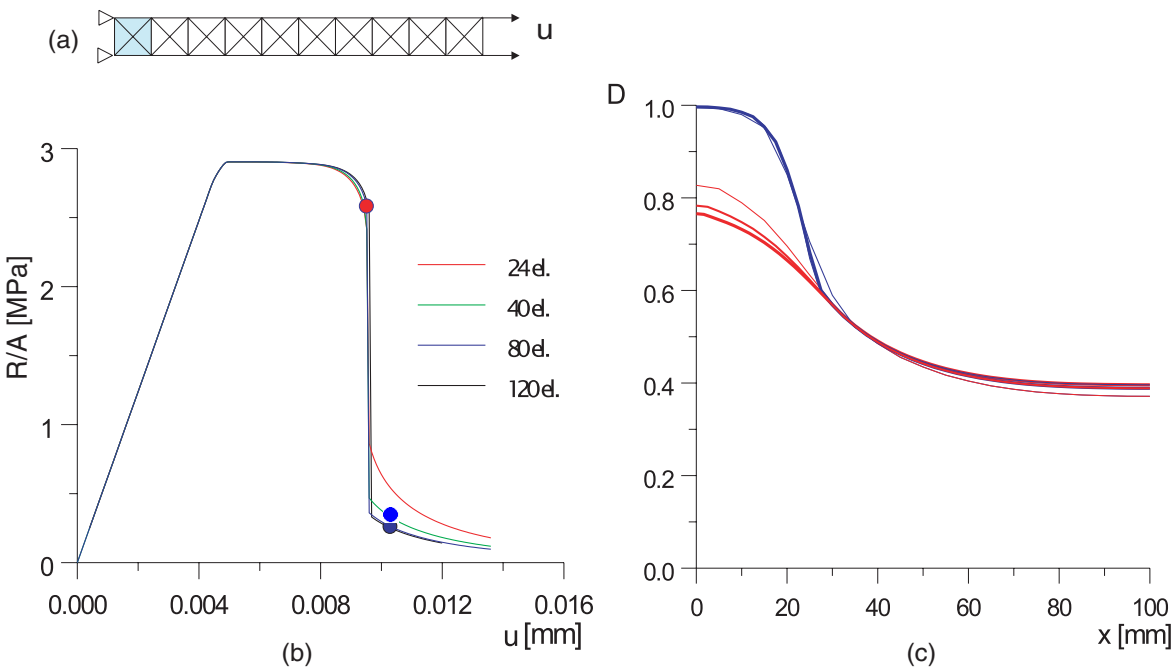

Figure 5: One-dimensional bar in tension: (a) geometry and FE discretization; (b) built-in end reaction stress versus imposed displacement for varying FE meshes; (c) damage distribution along the bar at the loading stages marked by the spots in (b).

nonlocally defined, while the damage variables remain locally defined, the only difference in the numerical solution of the finite step problem with respect to the usual iterative scheme used for the local inelastic models is the addition of an averaging phase between the predictor and the corrector phases. The input quantities of the corrector phase become the nonlocal strain invariants, but the evaluation of the updated damage values can be performed locally in the usual way.

The problem of the quasi-static response of a bar subject to the imposed displacement u of Fig. 5 is considered. The bar is discretized with four meshes of 24, 40, 80 and 160 three-nodes CST Finite Elements (in Fig. 5a the 40-elements mesh is shown); to trigger strain localization, the first shaded elements near the built-in end are slightly weaker with a reduced material parameter k_t.

Figure 5b shows the computed built-in end reaction divided by the nominal specimen section as a function of the imposed displacement as obtained for the four different FE discretizations. The different curves rapidly converge to a mesh independent solution, upon mesh refinement. The vertical after-peak drop of the reaction corresponds to the rapid damage growth which approaches the limit value 1 in the localized zone near the built-in end. The damage growth is rather unstable under displacement control for this uniaxial case.

The damage profiles at a stage right before the vertical drop of the reaction (red spot

in Fig. 5b) and at a state on the tail that develops after this drop (blue spot in Fig. 5b) are plotted in Fig. 5c for the three meshes with higher refinement; again, as the mesh is refined, convergence to a mesh-independent profile is observed.

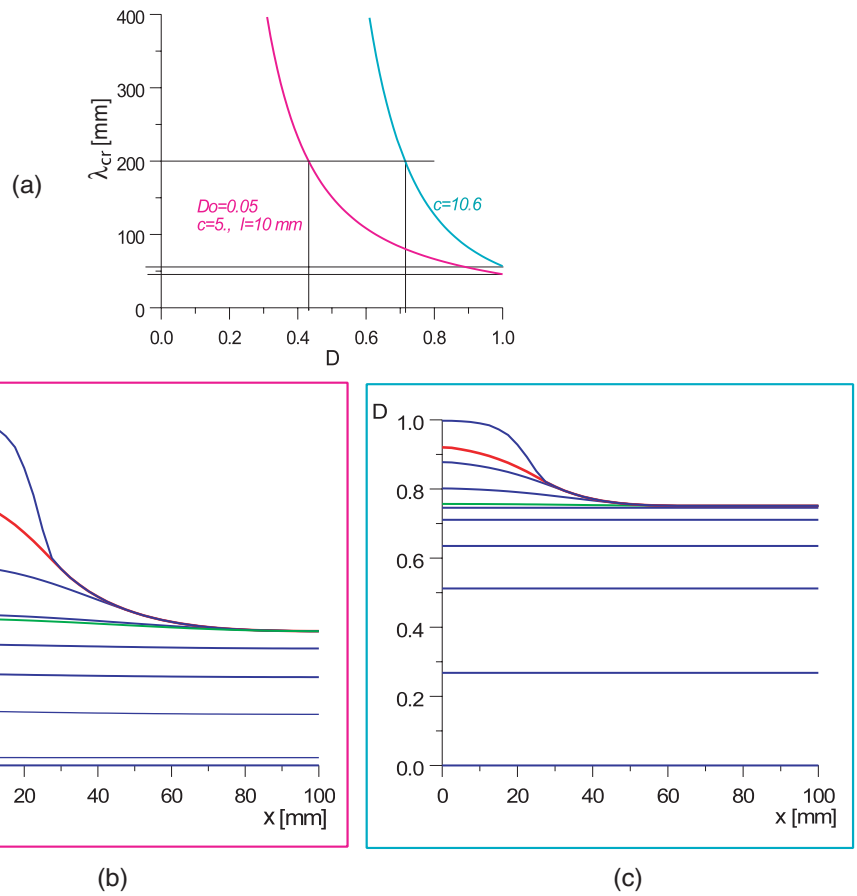

Figure 6: One-dimensional bar in tension: (a) characteristic length λ_{cr} vs damage D; (b) damage profiles for c=5; (c) damage profiles for c=10.6.

The influence of parameter c on the localization process, already discussed analytically (cfr Fig. 3b) is confirmed by the numerical analyses. Figures 6b and 6c show the evolutions of the damage profiles during the analyses for c=5 and c=10.6 , respectively, while Fig. 6a displays the analytically computed critical length vs damage curves for the same values of c.

To interpret the results note first that the numerical analyses have been carried out on a built-in-end bar in which localization was triggered at this end. This scheme can be thought of as half of a bar of length L^*=2 L=200 mm, symmetrically loaded and weakened at the center. From Fig. 6a one can see that the critical wave length λ_{cr}, representing the width of the localization zone, is bigger then twice the length L of the bar for low

values of damage, therefore at a first stage damage grows in the whole bar; namely, in the case c=5 (pink line) $\lambda_{cr} \geq 200$ mm for $D \leq 0.42$, while in the case c=10.6 (green line) $\lambda_{cr} \geq 200$ mm for $D \leq 0.7$. This is confirmed by the numerical analyses: localization within the bar, i.e. unloading in some elements, occurs when damage reaches the values $D \simeq 0.42$ and $D \simeq 0.7$, respectively (situations represented by the green profiles in Figs 6b and 6c). Then the localization zones shrink, to reach the predicted asymptotic value around 50 mm as damage tends to one; accordingly, the final profiles of damage in the built-in-end bar exhibit a localization zone of about 25 mm.

7 CONCLUSIONS

Some aspects of the bifurcation behavior of local and nonlocal damageable materials with different behaviors in tension and compression have been studied. In particular it has been shown that:

- Strain localization of the local model may happen in the hardening regime due to the nonassociativity of the material formulation. The onset of strain localization has been detected for different biaxial stress states in terms of critical localization directions and critical values of the damage variables at the localization onset. Localization may occur with in-plane or out-of-plane normal and is triggered for stress states sticked to the corners formed at the intersection of the two loading functions in the biaxial stress plane.

- The introduction of nonlocality in the loading functions has a regularizing effect in both enhanced versions, since it prevents the ill-posedness of the initial-boundary value problem and the consequent mesh-dependence of numerical results. The characteristic lengths implicitly introduced by the nonlocal models have been quantified analytically by means of a one-dimensional wave propagation analysis.

- Such internal lengths do depend on the values reached by the damage variables. For the assumed integral model, the characteristic length decreases as damage increases and tends to a finite, nonzero value, when damage tends to zero. For the gradient dependent model, different functional dependencies of the characteristic length with damage can be obtained by properly defining the diffusion functions which multiply the second-order gradient terms in the loading functions. These results have been confirmed by FE computations of the quasi-static response of a tensile bar by using the nonlocal damage model.

Acknowledgements

The authors would like to acknowledge financial support from the Italian Ministry (MURST).

REFERENCES

[1] M. Ortiz, "A constitutive theory for the inelastic behavior of concrete", *Mech. of Materials*, **4**,67-93 (1985).

[2] J.W. Ju, "On energy-based coupled elastoplastc damage theories: constitutive modeling and computational aspects", *Int. J. Solids Struct.* **23**(7), 803-833 (1989).

[3] J. Mazars and G. Pijaudier-Cabot, "Continuum damage theory. Application to concrete", *ASCE J. Engng. Mech.* **89**(2), 345-365 (1989).

[4] S. Ramtani, Y. Berthaud and J. Mazars, "Orthotropic behavior of concrete with directional aspects: modelling and experiments", *Nuclear Eng. Design*, **133**, 97-111 (1992).

[5] I. Carol, E. Rizzi and K. Willam, "A unified theory of elastic degradation and damage based on a loading surface", *Int. J. Solids Structures*, **31**(20), 2835-2865 (1994).

[6] C. Comi, Y. Berthaud and R. Billardon, "On localization in ductile-brittle materials under compressive loadings", *Eur. J. Mech. A/Solids*, **14**(1), 19-43 (1995).

[7] D. Halm and A. Dragon, "A model of anisotropic damage by mesocrack growth; unilateral effect", *Int. J. Damage Mech.*, **5**, 384-402 (1996).

[8] I. Carol, E. Rizzi and K. Willam, "On the formulation of anisotropic elastic degradation. Part I: Theory based on a pseudo-logarithmic damage tensor rate. Part II: Generalized pseudo-Rankine model for tensile damage", *Int. J. Solids Structures*, in press (2000).

[9] C. Comi, U. Perego, "A bi-dissipative damage model for concrete with application to dam engineering", *ECCOMAS 2000*, Barcelona, Spain, 11-14 September 2000, CD-ROM Proc. (2000).

[10] G. Maier and T. Hueckel, "Nonassociated and coupled flow rules of elastoplasticity for rock-like materials", *Int. J. Rock Mech. Min. Sci. & Geomech. Abstr.,* **16**, 77-92 (1979).

[11] A. Benallal, R. Billardon and G. Geymonat, "Some mathematical aspects of the damage softening problem", *Cracking and Damage*, J. Mazars and Z.P. Bažant Eds., Elsevier, Amsterdam, 247-258 (1988).

[12] D. Bigoni and T. Hueckel, "Uniqueness and localization. -I Associative and non-associative elastoplasticity. -II. Coupled elastoplasticity", *Int. J. Solids Structures*, **28**(2), 197-214, 215-224 (1991).

[13] E. Rizzi, I. Carol and K. Willam, "Localization analysis of elastic degradation with application to scalar damage", *J. Eng. Mech.*, ASCE, **121**(4), 541-554 (1995).

[14] B. Loret and E. Rizzi, "Anisotropic stiffness degradation triggers onset of strain localization", *Int. J. Plasticity*, **13**(5), 447-459 (1997).

[15] G. Pijaudier-Cabot and Z.L. Bažant, "Nonlocal damage theory", *J. Eng. Mech.*, ASCE, **113**, 1512-1533 (1987).

[16] M. Frémond and B. Nedjar, "Damage, gradient of damage and principle of virtual power", *Int. J. Solids Structures*, **33**(8), 1083-1103 (1996).

[17] R.H.J. Peerlings, R. de Borst, W.A.M. Brekelmans, J.H.P. de Vree and I. Spee, "Some observations on localization in non-local and gradient damage models", *Eur. J. Mech. A/Solids*, **15**(6), 937-953 (1996).

[18] C. Comi, "Computational modelling of gradient-enhanced damage in quasi-brittle materials", *Mechanics of Cohesive-Frictional Materials*, **4**(1), 17-36 (1999).

[19] C. Comi, "A nonlocal model with tension and compression damage mechanisms", submitted for publication (2000).

[20] J.W. Rudnicki and J.R. Rice, "Conditions for the localization of deformation in pressure-sensitive dilatant materials", *J. Mech. Phys. Solids*, **23**, 371-394 (1975).

[21] J.R. Rice, "The localization of plastic deformation", *Theoretical and Applied Mechanics*, 14th IUTAM Congress, Delft, W.T. Koiter Ed., North-Holland Publishing Company, Amsterdam, 207-220 (1976).

[22] G. Borré and G. Maier, "On linear versus nonlinear flow rules in strain localization analysis", *Meccanica*, **24**, 36-41 (1989).

[23] N.S. Ottosen and K. Runesson, "Properties of discontinuous bifurcation solutions in elasto-plasticity", *Int. J. Solids Struct.*, **27**(4), 401-421 (1991).

[24] E. Rizzi, G. Maier and K. Willam, "On failure indicators in multidissipative materials", *Int. J. Solids Structures*, **33**(20-22), 3187-3214 (1996).

[25] Z.P. Bažant and G. Pijaudier-Cabot, "Measurement of characteristic length of nonlocal continuum", *J. Appl. Mech.*, **115**, 755-767 (1989).

[26] D.C. Jansen and S.P. Shah, "Effect of length on compressive strain softening of concrete", *J. Eng. Mech*, ASCE, **123**, 25-35 (1997).

[27] A. Curnier, Q.-C. He and P. Zysset, "Conewise linear elastic materials", *J. of Elasticity*, **37**, 1-38 (1995).

[28] A. Benallal and C. Comi, "Localisation analysis via a geometrical method", *Int. J. Solids Structures*, **33**, 99-119 (1996).

[29] G. Pijaudier-Cabot and A. Benallal, "Strain localization and bifurcation in a non local continuum", *Int. J. Solids Structures*, **30**(13), 1761-1775 (1993).

[30] A. Benallal and V. Tvergaard, "Nonlocal continuum effects on bifurcation in the plane strain tension-compression test", *J. Mech. Phys. Solids*, **43**, 741-770 (1995).